In Situ Scanning Probe Microscopy of Interfacial Phenomena in Batteries

by Minoru Inaba, Soon-Ki Jeong, and Zempachi Ogumi

Scanning probe microscopy (SPM) is a type of microscopy that generates images of surfaces using a probe that scans (rasters) the specimen. SPM originates from the invention of scanning tunneling microscopy (STM) by Binnig and Rohrer in 1981.[1] They succeeded in imaging the (7 x 7) atomic structure on silicon (111) single crystal surface, and were awarded the 1986 Nobel Prize in Physics for their discovery. Atomic force microscopy (AFM), by which we can observe insulating surfaces, was developed by Binnig et al. in 1985,[2] and this invention extended widely the application of SPM. In addition to STM and AFM, a variety of probes in the SPM family have been developed recently. These include Kelvin probe force microscopy (KPFM), magnetic force microscopy (MFM), near-field scanning optical microscopy (NSOM), scanning electrochemical microscopy (SECM), scanning Hall probe microscopy (SHPM), and so on.

STM and AFM have very high resolution—high enough to obtain atomic-scale images of the surface. They can be used not only under high vacuum, but also in air or in solution. The last fact is a big advantage over electron microscopy for electrochemists who are interested in the phenomena taking place at electrode/electrolyte solution interfaces. In 1988, an electrochemical STM system coupled with dual potentiostat was already developed by Itaya et al.[3] Since then, *in situ* electrochemical STM and AFM have been used to analyze a variety of interfacial phenomena,[4,5] especially on single crystal surfaces.

In the field of batteries, *ex situ* STM and AFM are now widely used for characterizing the surface morphologies of samples. Though *in situ* SPM is not popularly used in the field of batteries at present, it is a powerful tool for analyzing interfacial phenomena in batteries because the interfaces can be directly observed. The authors have developed *in situ* STM and AFM techniques to analyze the interfacial phenomena in lithium-ion batteries (LIBs) since the early 1990s. Here we introduce some techniques essential to *in situ* observation and review our results obtained using *in situ* STM and AFM.

Techniques for *In Situ* SPM Observation

The details for the principles and equipment of STM and AFM have been published in the literature.[4,6] Here we introduce some important points essential to *in situ* SPM observation of interfacial phenomena in LIBs. The most important point is to use an SPM unit in an inert atmosphere where water and oxygen are strictly removed, because most of the active materials and their battery reactions are significantly affected by the presence of water and oxygen. The authors recommend that the SPM unit be placed in an argon glove box with water and oxygen content less than 1 ppm. For most LIB materials, the presence of water is more harmful than that of oxygen, and observation may be possible in a dry room with a dew point less than -40°C.

A vibration-free atmosphere is also important to obtain clear images with high resolution, and hence the SPM unit should be placed on an anti-vibration system in the glove box. Soundproofing from the outside of the glove box is not necessary, but noise and vibrations from the argon purification system often deteriorate the quality of the images. The gas circulation through the purification system should be suspended during SPM measurements; however, invasion of a small amount of oxygen and water is inevitable in measurements longer than a few hours.

Porous composite electrodes made of an active material powder, a carbon conductor, and a binder, coated on a metal current-collector (Cu or Al) are used in LIBs. However, in most cases, they cannot be used in SPM observation because the surface roughness is too large to detect subtle changes in morphology during charging and discharging. Model electrodes with smooth surfaces, e.g., thin film electrodes prepared by sputtering, vacuum deposition, electrodeposition, etc., can be used for *in situ* SPM measurements. Highly oriented pyrolytic graphite (HOPG), which has an atomically flat surface as shown in Fig. 1a, is often used as a model electrode for graphite negative electrode.

A typical cell for *in situ* AFM is shown in Fig. 1b The cell for *in situ* SPM measurements is simple, and can be constructed with a commercially available highly purified electrolyte solution and lithium foil as counter and reference electrodes. Though assembling the cell in the glove box requires some skill, most of the operation of the SPM unit is automatic in the latest SPM equipment.

Highly Oriented Pyrolytic Graphite

Charge/discharge properties, cycleability, durability of LIBs are significantly affected by the kind of electrolyte systems.[7] One of the reasons is attributable[7,8] to a passivating surface film, called solid electrolyte interface (SEI), that is formed on the graphite negative electrode. This film occurs by decomposition of the electrolyte solution upon the initial charging of LIBs.[7,8] The SEI prevents further solvent decomposition, and enables lithium ions to be intercalated within the graphite negative electrode. Most of the commercially available LIBs employ solvent systems based on ethylene carbonate (EC) as a primary solvent, because EC gives a stable and superior SEI. The SEI formation on graphite negative electrodes has been intensively investigated using *in situ* SPM methods.[9-14]

A freshly cleaved surface of HOPG was used as a model for graphite negative electrode to investigate the SEI formation. A typical STM image of HOPG basal plane is shown in Fig. 2a,[10] which was obtained at 2.8 V (» open-circuit potential) *vs.* Li^+/Li where no reaction takes place. A clear step of 3 nm in height is seen horizontally in the image, which corresponds to nine layers of graphene sheets. After the potential was kept at 1.1 V (Fig. 2b and 2c), part of the basal plane surface in the vicinity of the step edge was raised by about 1 nm. The authors called such features "hill-like" structures in their original papers.[10,11] It should be noted that an electronically insulating layer was not formed on the basal plane surface at 1.1 V, because we obtained these images by STM, which needs conductive surface for observation. The observed height of the hills was ca. 1 nm, which is comparable to interlayer spacings in stage 1 graphite intercalation compounds of alkali metals with organic solvent molecules, such as tetrahydrofuran (THF) and dimethoxyethane (DME). It is thus likely that these hills were formed by solvent

(continued on next page)

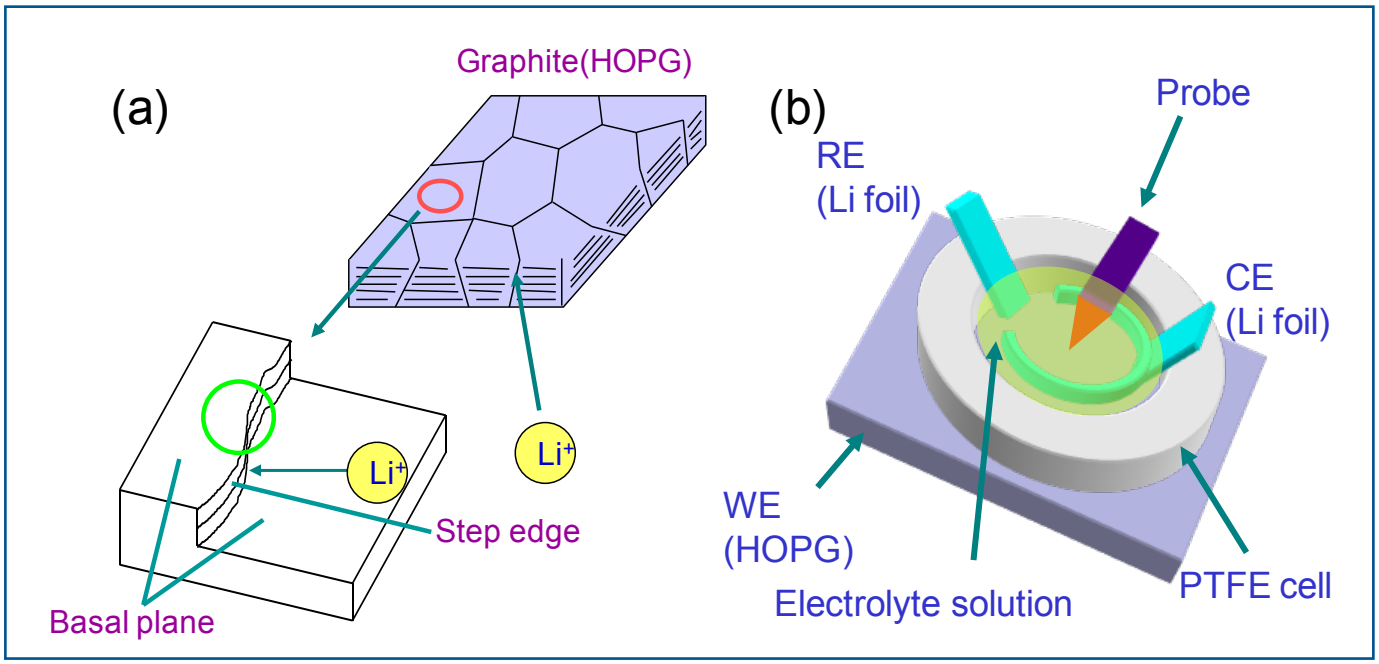

Fig. 1. *Schematic diagrams of (a) highly oriented pyrolytic graphite and (b) electrochemical cell for* in situ *SPM observation.*

co-intercalation (the intercalation of solvated lithium ion) at 1.1 V, which implies that solvent co-intercalation is involved in the initial processes of the SEI formation. Unfortunately clear images were not obtained at potentials more negative than ca. 1 V by STM. This fact indicated that an insulating surface layer is formed on the surface at potentials more negative than 1 V.

Figure 3 shows the results obtained by *in situ* AFM,[11] by which we could observe the surface covered with insulating film at potentials lower than 1 V. Panel (a) shows a cyclic voltammogram of HOPG basal plane at a slow scan rate of 0.5 mV s^{-1} between 2.9 and 0.0 V. In the first cycle, three major cathodic peaks appeared at ca. 1.0, 0.8, and 0.5 V, which are attributed to irreversible decomposition reactions of the electrolyte solution. AFM images (b) to (f) in Fig. 3 show morphology changes in a 5 x 5 μm area obtained during the first cycle in Fig. 2a. The arrows in parentheses denote the direction scanned by the micro-cantilever; for example, the top and bottom lines of Fig. 3c were obtained at 1.10 (top) and 0.95 V (bottom), respectively. AFM image (d) shows the morphology in the potential range of 0.95–0.80 V, and image (e) shows a magnified image of (d). A complicated pattern elevated by either 1 or 2 nm appeared on the basal plane surface in the potential region of 0.95-0.87 V. The elevated structures had atomically flat surfaces, and overlapped with one another. These structures are similar to the "hill-like" structures in Fig. 2, which were formed by solvent co-intercalation.

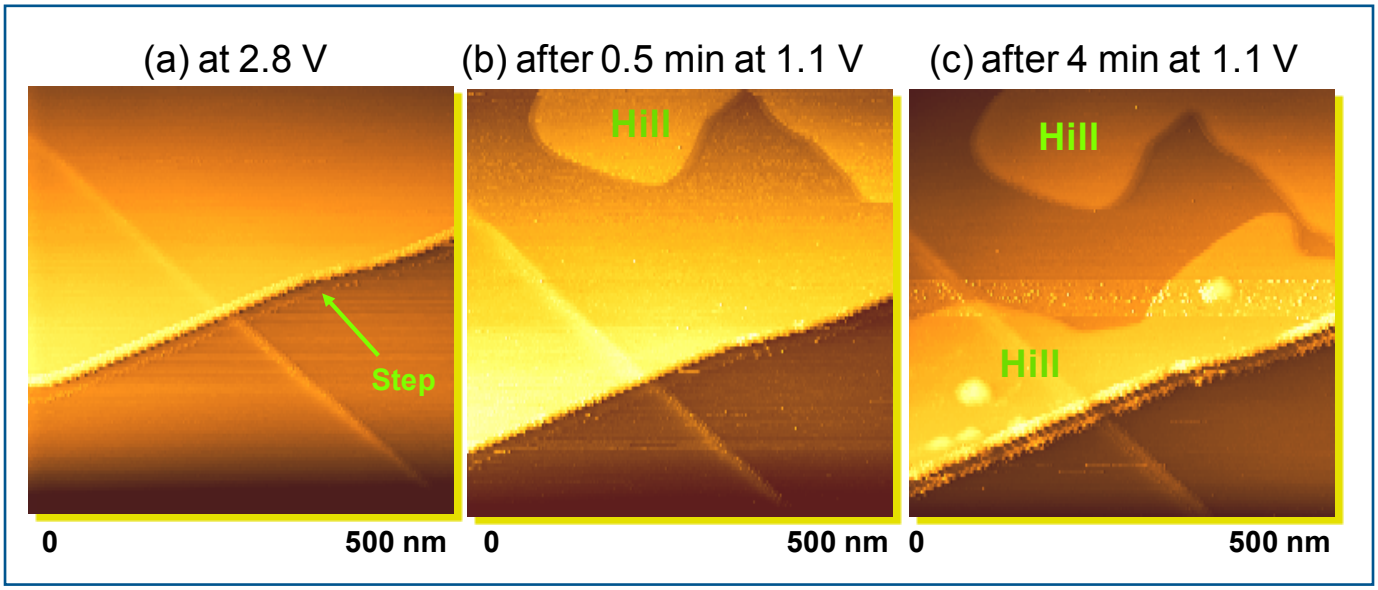

Fig. 2. *STM images (500 x 500 nm) of HOPG basal plane obtained (a) 2.9 V, and at (b) 0.5, (c) 4 min after the potential was stepped to 1.1V in 1 M $LiClO_4$/EC+DEC. The potential of the Pt/Ir tip was 3.0 V. (From Ref. 10. Reproduced with permission from The American Chemical Society.)*

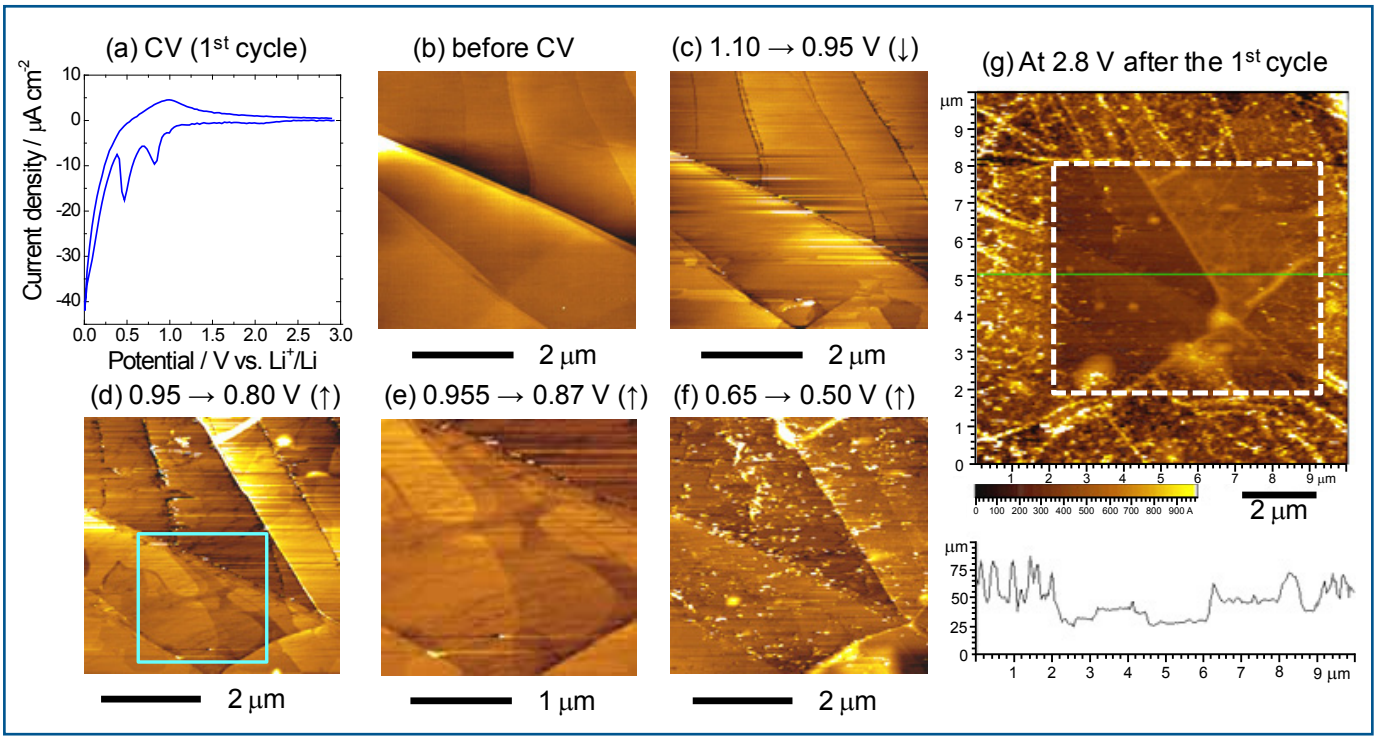

Fig. 3. *Cyclic voltammogram (a) and AFM images of the HOPG basal plane surface obtained at (b) 2.9 V before CV, (c) 1.10–0.95 V, (d) 0.95–0.80 V, (e) magnified image of the square in (d) (0.955-0.87 V), (f) 0.65–0.50 V during the first cycle at 0.5 mV s^{-1} in 1 M $LiClO_4$/EC+DEC (1:1), and (g) AFM image and height profile obtained at 2.9 V after the first cycle. The dotted rectangular shows the area observed by AFM during the first cycle. (From Ref. 11.)*

At potentials more negative than 0.65 V in Fig. 3f, particle-like precipitates appeared on the HOPG surface. The number of the precipitates increased with lowering the potential down to 0.0 V (not shown). The precipitates are considered to be decomposition products of solvent molecules, such as lithium alkoxides,[15] lithium alkyl carbonates,[15] and polymerized oligomers of EC.[16]

The precipitates formed at lower potentials were scraped off at 2.9 V by repeated AFM scanning in the contact mode. Figure 3g shows an AFM image and a height profile of an extended area (10 x 10 μm) including the 5 x 5 μm area observed during the first cycle. Many precipitates are clearly seen on the surface outside the 5 x 5 μm area, although they are almost completely scraped off inside the 5 x 5 μm area. In addition, many swellings (called "blisters") formed beneath the surface can be seen inside the 5 x 5 mm area. From the height profile, the thickness of the precipitate layer in Fig. 2g was roughly estimated to be 20-40 nm.

The results of AFM observation revealed that the SEI formation on graphite negative electrode involves the following two different processes: (i) the intercalation of solvated lithium ions and their decomposition beneath the surface at around 1 V and (ii) direct decomposition of solvents on the basal plane to form a precipitate layer at lower potentials. It is reasonable to think that the presence of the decomposition products (blisters) in the interlayer space of graphite prevents further solvent co-intercalation. On the contrary, the precipitate layer has a role in suppressing further reductive decomposition of solvent molecules on the basal plane.

Graphite Composite Electrode

Though *in situ* observation of composite electrode is usually difficult as mentioned earlier, we succeeded in observing the morphology changes of a composite electrode made of natural graphite flake powder as shown in Fig. 4.[14] At 1.1 V, swelling of the particle edges was observed (Fig. 4c), which indicates that solvated lithium ions were intercalated from the edges and decomposed inside the graphite particles in the vicinity of the edges. When charged to 0.0 V, the surfaces of graphite particles were covered thickly with decomposition products of the solvents. These phenomena are in good agreement with the SEI forming processes discussed in the previous section.

Sn Thin Film Electrode

Metals such as Sn and Si make alloys with lithium metal, and hence are expected as high capacity negative electrodes because their theoretical capacities are much higher than graphite (994 and 4200 mAh g^{-1}, respectively). However, poor cycleability is one of big disadvantages of the Li-alloy electrodes. Figure 5 shows cyclic voltammograms and *in situ* AFM images of a Sn thin film (1 μm thick) prepared by electroplating.[17] The cathodic peak at ca. 0.25 V and the anodic peak at ca. 0.7 V correspond to alloying and de-alloying of lithium with tin. Both peaks significantly decreased with cycling. The surface of the Sn thin film was smooth before cycling; however, it became very rough after cycling. Such surface roughing was caused by expansion and shrinkage during alloying and de-alloying, respectively, and was the reason for the capacity fade upon cycling.

The irreversible cathodic peak at ca. 1.2 V is attributable to solvent decomposition and SEI formation on Sn. It should be noted that the irreversible peak was scarcely observed in the first cycle, but greatly enhanced in the second and third cycle. The morphology change after the first and the second cycle was more remarkable than after the third or later cycle, and hence a significant increase in surface area in the first and second cycle may be the reason for the enhanced irreversible reactions at ca. 1.2 V.

$LiMn_2O_4$ Thin Film Electrode

For *in situ* SPM analysis of positive electrode surfaces, thin films with flat surfaces, which are prepared by RF sputtering, pulsed laser deposition (PLD), etc., are often used as model electrodes, though there have been much fewer reports on positive electrodes. Figure 6 shows *in situ* AFM images of spinel

(continued on next page)

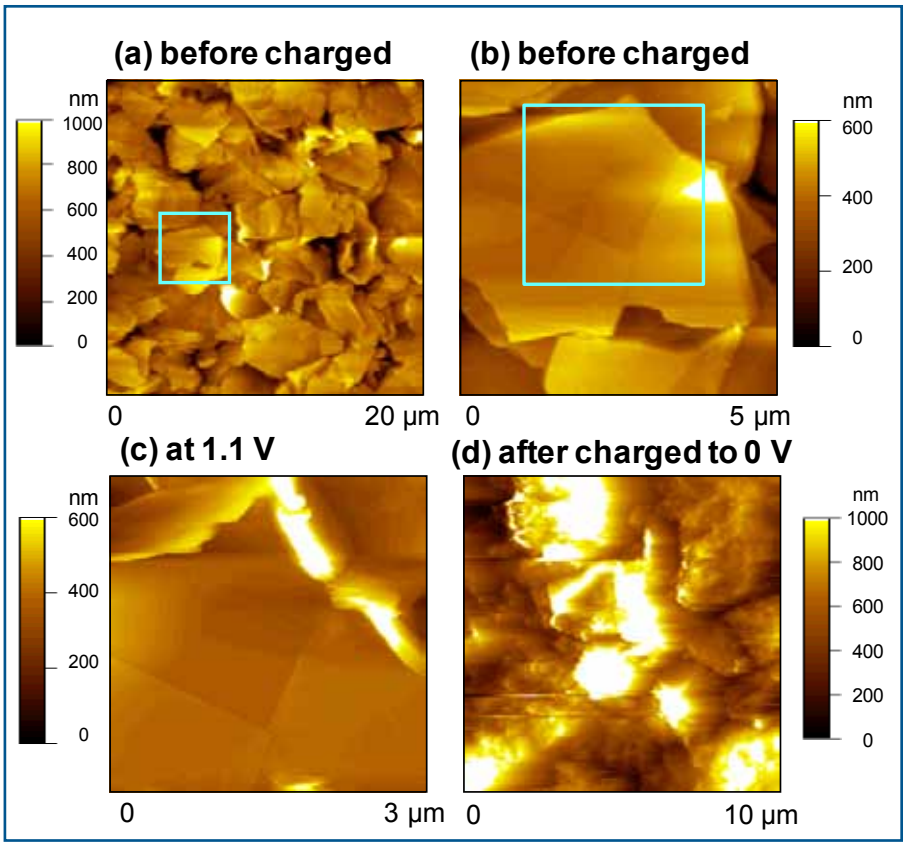

Fig. 4. *AFM images of the composite graphite (NG-7) electrode surface obtained at (a, b) the open circuit potential (~3.3 V), and (c) 1.1 V during constant current charging at 30 μA cm^{-2} and (d) after charged to 0.0 V in 1 M $LiClO_4$/EC+DEC. (a) 20 x 20 μm^2; (b) 5 x 5 μm^2; (c) 3 x 3 μm^2; (d) 10 x 10 μm^2. The squares in (a) and (b) shows the observed areas in (b) and (c), respectively. (From Ref. 14. Reproduced with permission from Elsevier, Ltd.)*

$LiMn_2O_4$ thin film electrodes prepared by PLD before and after potential cycles between 3.50 and 4.30 V.[18] Before cycling, the film consisted of fine particles of 80-100 nm in diameter (Fig. 6a and 6c). When the potential was cycled at 25°C, no appreciable morphology changes were observed even after 90 cycles (Fig. 6b). However, a significant change in morphology was observed at 60°C. Smaller particles of 20 nm in diameter appeared and some cavities were formed on the surface after 60 cycles (Fig. 6d). Though it is not clear why these morphology changes took place at 60°C, they are closely related with the capacity fade of $LiMn_2O_4$ positive electrodes at elevated temperatures. Further detailed AFM analysis revealed that these morphology changes are more significant in the lower potential region (3.50-4.04 V) of the working potential range of $LiMn_2O_4$ (3.50-4.30 V). These morphology changes may be correlated with the structural instability of $LiMn_2O_4$ at a depth of discharge (DOD) of ca. 75%,[19] though further investigation is needed.

Concluding Remarks

As the proverb "*Seeing is believing*" says, *in situ* SPM enables us to observe directly the electrode/electrolyte interface and therefore is a powerful technique for understanding interfacial phenomena in LIBs. Understanding the interfacial phenomena is a key to the development of innovative active materials and solvent systems for LIBs. There has been a remarkable improvement in commercially available SPM equipment for the past two decades, and even beginners can observe surface morphology of battery materials with a high resolution by SPM. The authors hope that *in situ* SPM will be used for the analysis of a variety of battery materials and interfacial reactions by many researchers in the near future.

About the Authors

Minoru Inaba is a professor in the Department of Molecular Chemistry and Biochemistry, Faculty of Science and Engineering, Doshisha University, Kyoto, Japan. He received his BSc from the Faculty of Engineering, Kyoto University in 1984, and his MSc (1986) and Dr. Eng. (1995) from the Graduate School of Engineering, Kyoto University. He has worked on electrochemical energy conversion systems including lithium-ion batteries and fuel cells. He may be reached at minaba@mail.doshisha.ac.jp.

Soon-Ki Jeong received his MS degree in industrial chemistry engineering from Hanyang University, Seoul, Republic of Korea in 1996; and his PhD in energy and hydrocarbon chemistry from Kyoto University, Japan in 2002. He is currently an associate professor in the Department of Chemical Enegineering at the Soochunhyang University, Asan, Republic of Korea. His current research mainly includes the area of interfacial reactions between the electrode and electrolyte in lithium secondary batteries. He may be reached at hamin611@sch.ac.kr.

Zempachi Ogumi retired from the Graduate School of Engineering, Kyoto University, Japan in 2009, and is currently a project manager of a NEDO RISING battery project focusing on the innovation of batteries as an adjunct professor at the Office of Society-Academia Collaboration for Innovation, Kyoto University. He received his PhD from Kyoto University. He is a Fellow of The Electrochemical Society. He may be reached at ogumi@scl.kyoto-u.ac.jp.

References

1. G. Binnig, H. Rohrer, Ch. Gerber, and E. Weibel, *Phys. Rev. Lett.*, **50**, 120 (1983).
2. G. Binnig, C. F. Quate, and Ch. Gerber, *Phys. Rev. Lett.*,**56**, 930 (1986).
3. K. Itaya and E. Tomita, *Surf. Sci.*, **201**, L507 (1988).
4. A. A. Gewirth and B. K. Niece, *Chem. Rev.*, **97**, 1129 (1997).
5. S. Kalinin and A. Gruverman, Eds., *Scanning Probe Microscopy: Electrical and Electromechanical Phenomena at the Nanoscale*, Springer, New York (2006).
6. D. Bonnel, Ed., *Scanning Probe Microscopy and Spectroscopy: Theory, Techniques, and Applications*, 2nd ed., Wiley-VCH, New York (2001).
7. Z. Ogumi and M. Inaba, *Bull. Chem. Soc. Jpn.*, **71**, 521 (1998).
8. E. Peled, in *Handbook of Battery Materials*, J. O. Besenhard, Ed., pp. 419-458, Wiley-VCH, Weinheim (1999).

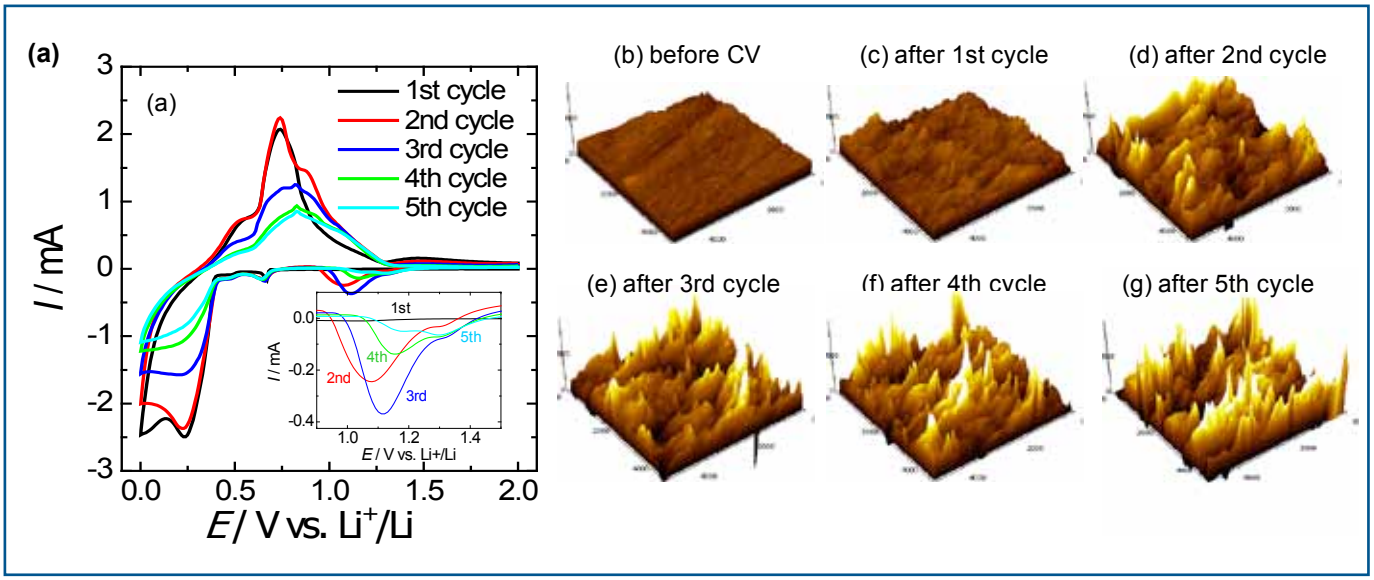

Fig. 5. *Cyclic voltammograms (a) of Sn thin film at 0.5 mV s^{-1} between 2.0 and 0.0 V in 1 M $LiClO_4$/PC and AFM images (b-g, 5 x 5 μm) before cycling and after (c) 1, (d) 2, (e) 3, (f) 4, and (g) 5 cycles obtained at 2.0 V. The inset in (a) is a magnified voltammogram in the range of 0.9-1.5 V. (From Ref. 17. Reproduced with permission from Elsevier, Ltd.)*

9. D. Allita, R. Kotz, P. Novak, and H. Siegenthaler, *Electrochem. Commun.*, **2**, 436 (2000).
10. M. Inaba, Z. Siroma, A. Funabiki, Z. Ogumi, T. Abe, Y. Mizutani, and M. Asano, *Langmuir*, **12**, 1535 (1996).
11. M. Inaba, Z. Siroma, Y. Kawatate, A. Funabiki, and Z. Ogumi, *J. Power Sources*, **68** (1997) 221.
12. S.-K. Jeong, M. Inaba, T. Abe, and Z. Ogumi, *J. Electrochem. Soc.*, **148**, A989 (2001).
13. S.-K. Jeong, M. Inaba, R. Mogi, Y. Iriyama, T. Abe, and Z. Ogumi, *Langmuir*, **17** (2001) 8281.
14. S.-K. Jeong, M. Inaba, Y. Iriyama, T. Abe, and Z. Ogumi, *J. Power Sources*, **119-121**, 555 (2003).
15. Y. Ein-Eli, B. Markovsky, D. Aurbach, Y. Carmeli, H. Yamin, and S. Luski, *Electrochim. Acta*, **39**, 2559 (1994).
16. Z. Ogumi, A. Sano, M. Inaba, and T. Abe, *J. Power Sources*, **97-98**, 156 (2001).
17. M. Inaba, T. Uno, and A. Tasaka, *J. Power Sources*, **146**, 473 (2005).
18. T. Doi, M. Inaba, H. Tsuchiya, S. K. Jeong, Y. Iriyama, T. Abe, and Z. Ogumi, *J. Power Sources*, **180**, 539 (2008).
19. G. Li, Y. Iijima, Y. Kudo, and H. Azuma, *Solid State Ionics*, **146**, 55 (2002).

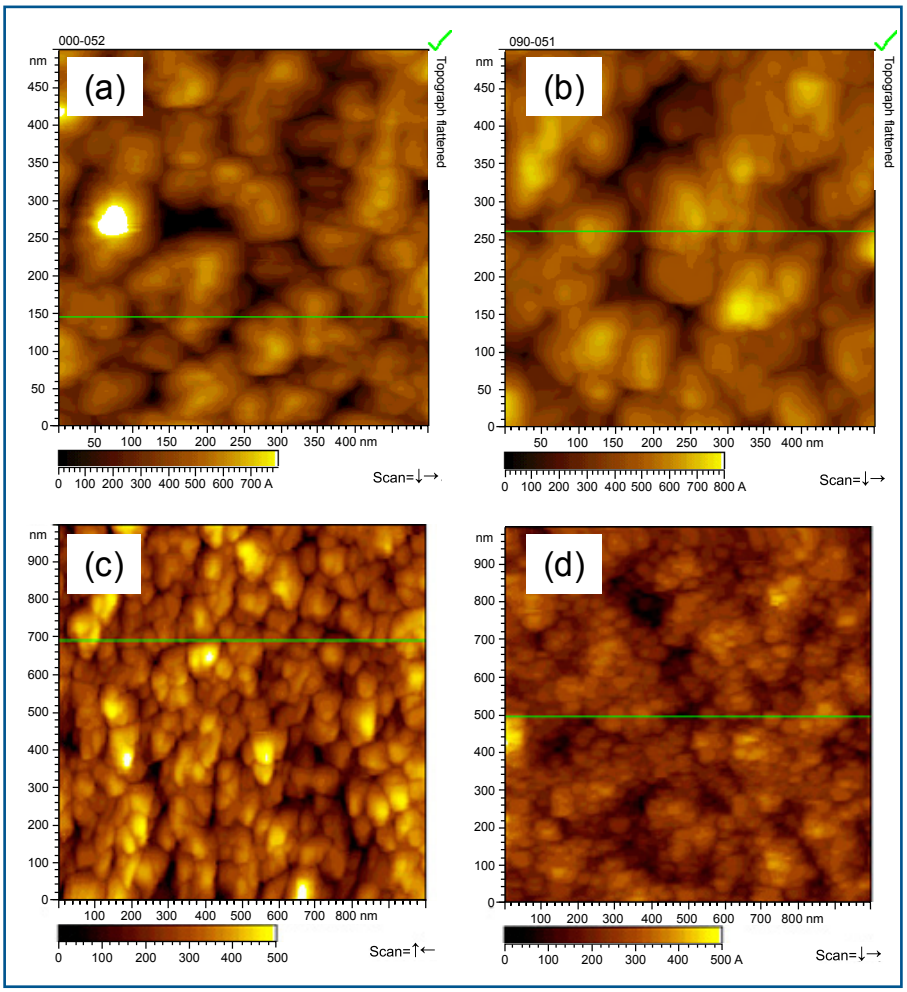

Fig. 6. *AFM images of $LiMn_2O_4$ thin films prepared by pulsed laser deposition before and after potential cycling at 1 mV s^{-1} between 3.50 and 4.30 V in 1 M $LiPF_6$/PC. (a, b) 500 x 500 nm at 25°C, (c, d) 1 x 1 μm at 60°C. (a, c) before cycling, (b) after 90 cycles, (d) after 60 cycles. (From Ref. 18. Reproduced with permission from Elsevier, Ltd.)*